ELSEVIER

International Journal of Heat and Fluid Flow 20 (1999) 1–9

International Journal of HEAT AND FLUID FLOW

Numerical study of turbulent heat transfer in confined and unconfined impinging jets

M. Behnia [a,*], S. Parneix [a], Y. Shabany [b], P.A. Durbin [b]

[a] *Center for Turbulence Research, Stanford University, MS 202A-1, Stanford, CA 94305-3030, USA*
[b] *Mechanical Engineering Department, Stanford University, Stanford, CA 94305-3030, USA*

Received 4 February 1998; accepted 30 June 1998

Abstract

An elliptic relaxation turbulence model ($v^2 - f$ model) has been used to simulate the flow and heat transfer in circular confined and unconfined impinging jet configurations. The model has been validated against available experimental data sets. Results have been obtained for a range of jet Reynolds numbers and jet-to-target distances. The effects of confinement on the local heat transfer behavior has been determined. It has been shown that confinement leads to a decrease in the average heat transfer rates, but the local stagnation heat transfer coefficient is unchanged. The effect of confinement is only significant in very low nozzle-to-plate distances ($H/D < 0.25$). In contrast, the flow characteristics in the nozzle strongly affects the heat transfer rate, especially in the stagnation region. Quantitative (up to 30% difference) and qualitative differences have been obtained when different nozzle velocity profiles were used.

1. Introduction

In the last two decades, jet impingement heat transfer has received considerable attention in many industrial and engineering applications (e.g. manufacturing, material processing and electronic cooling). This has been due to the high heat transfer rates of jet impingement. There are numerous papers dealing with this problem both numerically and experimentally. A number of reviews have also appeared, amongst which some of the more recent are Jambunathan et al. (1992), Viskanta (1993) and Webb and Ma (1995).

There are a number of parameters which can affect the heat transfer rate in a jet impingement configuration. For instance, the jet-to-target distance not only affects the heat transfer rate, but also has a significant effect on the local heat transfer coefficient distribution (Baughn and Shimizu, 1989). For the design and optimization of jet impingement cooling or heating systems, it is essential that the effects of these important parameters are identified and understood. In some of previous studies these effects have been examined; however, experiments performed by different investigators have sometimes been contradictory, due to the differences in the experimental conditions. In their review, Jambunathan et al. (1992) clearly point out this problem and note that for a better understanding of the jet impingement heat transfer process, the details of the flow, geometry and turbulence conditions are required; only then can a comparison be made between different experimental data sets.

Due to the difficulties in performing and comparing experiments, a numerical study of the problem holds promise for quantifying the effects of the various parameters of interest. However, turbulent impinging jets have complex features due to entrainment, stagnation and high streamline curvature. These features prove to be somewhat difficult to represent with most existing turbulence models which are essentially developed and tested for flows parallel to a wall. Craft et al. (1993) have demonstrated some of the problems in these turbulence models; most importantly they obtained a substantial overprediction of the heat transfer in the stagnation region with a widely used low Reynolds number $k - \varepsilon$ turbulence model. Due to its complexity, this flow has been chosen as a challenging test-case (see ERCOFTAC database at http://www-fluindigo.mech.surrey.ac.uk) for the validation of turbulence models. A number of investigators have gauged the success of their models on this flow. However, turbulence modelers encounter numerous difficulties due either to the fact that the details of most of these experimental data sets are not known, or to the fact that the geometry and boundary conditions are not well posed.

We have used a few experimental data sets on axisymmetric turbulent jets impinging on a flat plate or a pedestal (see the configurations on Fig. 1) to validate the $v^2 - f$ turbulence model. For this purpose, we chose those data obtained in a fully developed impinging jet configuration (i.e. Baughn and Shimizu, 1989; Baughn et al., 1991; Baughn et al., 1993; Lytle and Webb, 1994; Yan, 1993; Mesbah, 1996). Subsequent computations were performed to assess effects of important parameters such as jet-to-target distance, geometry and Reynolds number, as well as to examine the influence of jet confinement and nozzle-exit profiles.

* Corresponding author. E-mail: M.Behnia@unsw.edu.au

0142-727X/99/$ – see front matter
PII: S0142-727X(98)10040-1

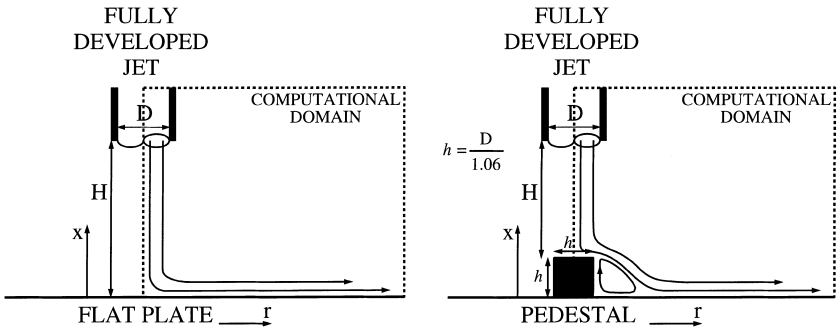

Fig. 1. Configuration and computational domain for the impinging jet on (a) flat plate and (b) a pedestal.

Published experimental data sets. Numerous experimental studies of jets impinging on surfaces have been undertaken. Some of these studies are noted in the review articles mentioned previously. The first experiments go back to the 1960's (see Jambunathan et al., 1992). With the advent of modern measurement and optical techniques, detailed flow and temperature fields have been obtained in the most recent experimental studies (see Viskanta, 1993; Webb and Ma, 1995). Unfortunately, due to the sensitive nature of these experiments, the data obtained by different investigators shows rather significant differences in the rates of heat transfer. This is despite the fact that most investigators have reported experimental uncertainties on the order of 5%. The data scatter may be partially due to the difference in jet outlet conditions, nozzle geometry, thermal boundary conditions, target plate geometry and experimental techniques. This has hindered the interpretation of these data both for understanding the pertinent physical phenomena, and for developing general heat transfer correlations.

We selected some of the most recent experiments on circular jets impinging on a flat plate (Fig. 1) for the validation of our numerical model. The local heat transfer rate on the impinging surface for a jet Reynolds number of 23,000 and a target-to-plate distance of 6 jet diameters, is shown in Fig. 2. The Re number is based on the jet outlet bulk velocity and the jet diameter. For a heated wall the Nusselt number can be written $D\partial_x T_w/T_w$ where T_w is the wall temperature relative to the jet temperature. This is essentially the dimensionless temperature gradient. Baughn and Shimizu (1989) used a uniformly heated plate in conjunction with liquid crystals for temperature distributions. The jet issued from a long pipe (72 diameters) and they noted that this provided a "nearly fully developed flow at the jet exit". Baughn et al. (1991) used the same experimental apparatus and technique to study entrainment effects. However, their baseline Nusselt number, which corresponds to the conditions of Baughn and Shimizu, is somewhat different (see Fig. 2). Yan (1993) used the same experimental apparatus and conditions as the other two studies. However he developed a liquid crystal, preheated-wall, transient technique that is amenable to more complex geometries. Again, the data is slightly different. Lytle and Webb (1994) focussed their study on low nozzle-to-plate spacings, but they also measured the widely-used distance of 6 diameters. Lytle and Webb used an infrared thermal imaging technique for temperature measurements. They have also reported some LDV flow measurements. They used two different pipes of 7.8 and 10.9 mm diameter, both with a 1.4 mm wall thickness and a 610 mm length. They noted that this ensured "fully developed flow over the Reynolds number range investigated". Their data is consistently somewhat higher than the other sets (see Fig. 2). Colucci and Viskanta (1996) studied a confined geometry with the jet issued from a nozzle machined in a plate. They used a thermochromatic liquid crystal technique to visualize and record isotherms on the uniformly heated impingement surface. They have reported their data at a Reynolds number of 20,000; however, in Fig. 2, the data has been rescaled by $Re^{0.7}$ (correlation proposed by Jambunathan et al., 1992). Their data plotted here is for a uniform diameter orifice with a slightly rounded entrance. It is noted that their Nu distribution, although for a substantially different jet outlet condition and despite the confinement, falls within the band of the above mentioned unconfined jet data.

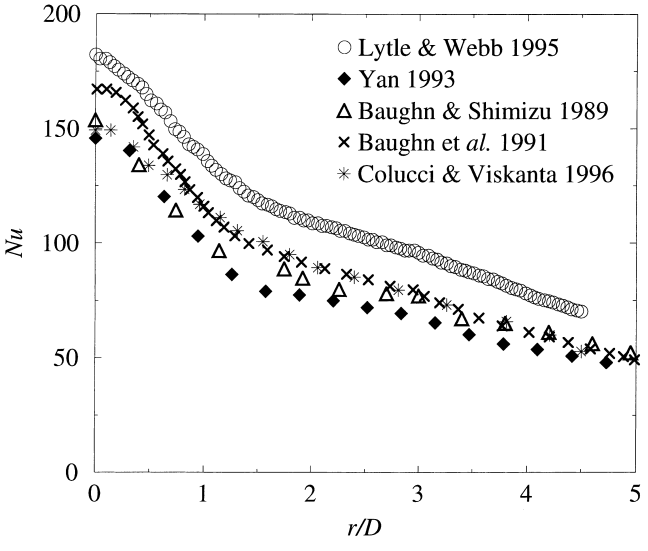

Fig. 2. Nusselt number for the impinging jet on the flat plate at Re = 23,000 and $H/D = 6$ from different experiments.

In conclusion, for the jet-to-plate distance of 6 jet diameters, Fig. 2 indicates that, at least for a Reynolds number of around 20,000, the confinement and the jet-outlet conditions have a marginal influence on the rate of heat transfer. However, for lower aspect ratios, the data indicates a somewhat stronger dependance on the geometry and flow conditions. For instance, at $H/D = 1$, the data of Colucci and Viskanta (1996) shows a local minimum in the stagnation region with two well pronounced peaks downstream of it (see Fig. 3). The results of Lytle and Webb (1994) show that the Nusselt number is maximum in the stagnation region, and away from it, decreases to a local minimum and then goes through a single peak. Also, for these low aspect ratios, Lytle (1990) noted that there is a slight dependance on the pipe diameter (this has also been observed by Garimella and Rice (1995)).

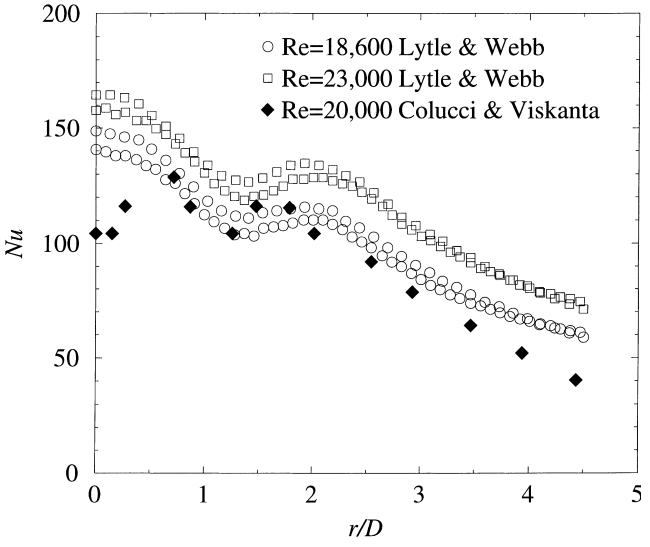

Fig. 3. Nusselt number for the impinging jet on the flat plate at $H/D = 1$ from different experiments.

2. Numerical procedure

2.1. Turbulence model

Most predictions of jet impingement heat transfer in industry involve the use of standard or modified versions of the $k-\varepsilon$ turbulence model, available in many existing CFD packages. These models have usually been developed, calibrated and validated using flows parallel to the wall. Physical phenomena involved in impinging flows on a solid surface are substantially different and have been considered as highly challenging test-cases for the validation of turbulence models. For example, $k-\varepsilon$ simulations performed by Craft et al. (1993) in a non-confined impinging jet cooling a heated flat plate showed dramatically poor results for wall heat transfer coefficients (e.g. more than 100% over-prediction in the stagnation region).

In order to integrate $k-\varepsilon$ to the wall, it is common practice to introduce low-Reynolds number damping functions. These are tuned to mimic certain near-wall behaviors (Launder and Sharma, 1974). However, all these models use a single-point approach that cannot represent the non-local effects of pressure-reflection that occur near solid boundaries. In many cases these damping functions involve an ill-defined normal distance to the wall, which cannot be used in complex geometries. They are also highly non-linear and sometimes introduce numerical stiffness.

An attractive alternative to the $k-\varepsilon$ model is the v^2-f turbulence model (Durbin, 1991). The model equations are outlined in the Appendix.

The v^2-f model could be thought of as a simplification of a full Second Moment Closure (SMC) model (Durbin, 1993). For instance, the source terms in Eq. (A.6) of Appendix A represent return to isotropy and isotropization models for energy redistribution. In this and other ways, important effects of near-wall anisotropy are represented. However, the v^2-f model has the advantage of solving the mean flow with an eddy viscosity, which avoids some computational stability problems encountered with the full SMC models. It is a general geometry turbulence model, valid right up to solid walls. It does not need wall functions whose universality is increasingly being called into question, especially in impinging regions.

The v^2-f model is based on certain physical concepts. It introduces a new velocity variance scale, $\overline{v^2}$ (instead of k), for the evaluation of the turbulent viscosity. In general $\overline{v^2}$ should be regarded as a scale for the velocity component responsible for turbulent transport. It is proportional to k far from solid walls, while in the near-wall region, it becomes the velocity fluctuation normal to the solid surface, irrespective of the orientation of the surface. Theoretically, k is unable to represent the damping of turbulent transport close to the wall, whereas normal velocity fluctuations provide the right scaling (Behnia et al., 1998).

Following a full Reynolds stress analysis (Durbin, 1993), and in order to model non-local characteristics of the near-wall turbulence without the use of two-point correlations, the v^2-f model uses an elliptic operator to compute a term analogous to the pressure-strain correlation. Ellipticity is introduced by a modified Helmholtz operator, which is amenable to numerical computations. It introduces wall effects by a linear equation. This operator generates turbulence profiles that evolve from the near-wall behavior to forms suitable for far from the solid boundaries. Finally, a mathematical constraint has been added to prevent non-realizability of the eddy viscosity especially in the stagnation region (Durbin, 1996).

The temperature field is computed through a standard eddy diffusivity approximation. A constant temperature boundary condition is used on the impingment walls. The Kays and Crawford formula (Kays and Crawford, 1993) for the turbulent Prandtl number, Pr_t, was chosen for all computations including $k-\varepsilon$. This formula gives a reasonable representation of data on Pr_t near the wall, it increases from 0.85 in the far-field to about 1.7 near the surface, and it yields somewhat better agreement in the impingement region. However, the improvement over using a constant $\mathrm{Pr}_t = 0.9$ is only on the order of 10% (Behnia et al., 1998); Pr_t variations cannot explain the 100% error of the $k-\varepsilon$ model.

2.2. Numerical method

The flow and the turbulent fields have to be accurately resolved to obtain good heat transfer predictions. All computations were performed in cylindrical coordinates with a general geometry, finite difference code developed by Rogers and Kwak (1990). The spatial discretization of convective terms was via a third order, upwind biased scheme; diffusion terms were central differenced. Fine, non-uniform, orthogonal, cylindrical grids were used, with a high resolution near all solid boundaries. A mesh sensitivity was carried out by halving the mesh spacing in the axial and radial directions. In all cases the first grid point was at $y_+ \approx 1$ or less. This changed the impingement region Nusselt number by less than 1%. Therfore, the solutions presented here are considered grid independent.

The flow conditions at the nozzle exit may affect the computed flow field. Therefore, for validation purposes, we chose the case of a jet being issued from a long pipe, so that nozzle-exit conditions are fully turbulent and well defined. A fully developed turbulent pipe flow was first computed in a preliminary computation, and then interpolated onto the full grid to provide the inlet condition of the jet. The computational domain began 1 to 2 pipe diameters upstream of the jet exit (depending on H/D), so that the pipe flow profiles may evolve in the nozzle as the flow approaches the nozzle outlet. It is noted that prescribing the inlet conditions upstream of sharp corners is also a requirement in other flows, e.g. the backward-facing step. In the unconfined case, this allows the upper computational boundary to be a sufficient distance from the wall so that it does not affect the flow near the impingement surface. Two values of the pipe wall thickness were examined, 0.112 D and 0.0313 D, corresponding to the experiments of

Baughn and Shimizu (1989) and Cooper et al. (1993) respectively. No noticeable difference was observed. The former value was used for the computations.

Grids of 120×120 nodes provide adequate resolution. Several computations with 240×240 nodes were done to verify this.

3. Model validation

3.1. Heat transfer coefficient

Computations were first performed for the widely used test-case of an unconfined impinging jet on a flat plat at $\mathrm{Re} = 23{,}000$ and for a nozzle-to-plate distance of 6 jet diameters. Fig. 4 shows that the distribution of the local heat transfer coefficient is fairly well reproduced by the $v^2 - f$ model. In fact, the simulation falls into the range of available experimental data sets, represented by the gray zone. The low Reynolds number $k - \varepsilon$ model significantly overpredicts the heat transfer rates in the stagnation region (by about 100%). This simulation was performed with a similar set of damping functions to those used in the Launder and Sharma model (1974). The results obtained by Craft et al. (1993) with precisely this later model showed a similar dramatic overprediction in the impinging region. This overestimation extends up to 2–3 jet diameters away from the stagnation point, although the flow has already become parallel to the surface at this location. This indicates that the quantitative inaccuracy spreads into the region surrounding the impinging area, which in turn may influence the whole distribution of heat transfer, even qualitatively.

The excellent $v^2 - f$ results are confirmed by studying the influence of the nozzle-to-target spacing, H/D, on the stagnation Nusselt number. Behnia et al. (1998) contains results similar to Fig. 4 for a nozzle-to-plate distance of 2 diameters. A more comprehensive parameter study has now been performed: a set of 15 computations was done for each model. The results are compared to the available experimental data sets in Fig. 5. The $v^2 - f$ model is in very good agreement with the experimental curve of best fit, yielding a maximum stagnation heat transfer rate at $H/D = 6$–7. Note that this optimal value has already been reported in numerous experimental studies (e.g. Martin, 1977; Baughn and Shimizu, 1989; Webb and Ma, 1995). The quantitative overprediction of the $k - \varepsilon$ model is present for all nozzle-to-plate spacings. If one wants to use this model for design purposes, the efficiency of the cooling system would be overestimated. More dramatically, the design optimization process would also fail completely. For instance, the $k - \varepsilon$ model predicts 2 optimal nozzle-to-plate distances of 2.5 and 5 diameters, in disagreement with the experiments.

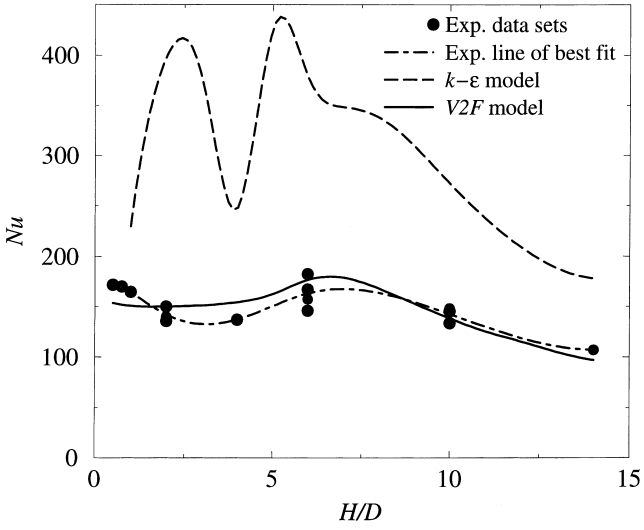

Fig. 5. Dependence of stagnation Nusselt number on nozzle-to-plate distance for the impinging jet on the flat plate at $\mathrm{Re} = 23{,}000$.

Fig. 6 shows the local wall heat transfer distribution in the case of an impinging jet on a wall-mounted pedestal. The same parameters ($\mathrm{Re} = 23{,}000$ and $H/D = 6$) have been chosen for this validation. As for the flat plate, $k - \varepsilon$ heat transfer predictions are more than 100% higher than the experiment. Moreover, the qualitative trend also fails, with a prediction of a local maximum at the stagnation point, whereas the experiment shows a local minimum. This erroneous behavior diffuses

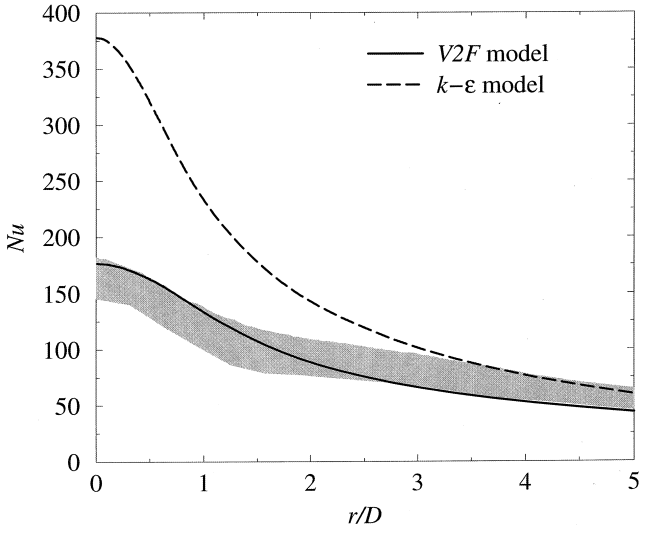

Fig. 4. Simulated Nusselt number distribution for the impinging jet on the flat plate at $H/D = 6$ and $\mathrm{Re} = 23{,}000$ (the shaded zone is the band of experimental data sets).

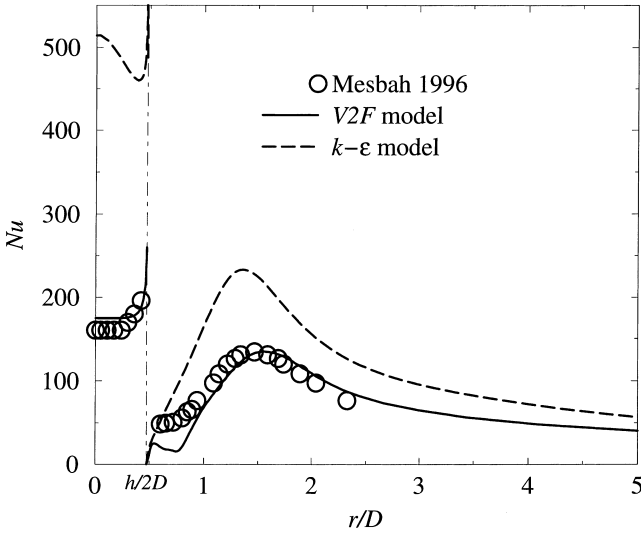

Fig. 6. Nusselt number distribution on top of the pedestal and downstream of it, on the plate, at $H/D = 6$ and $\mathrm{Re} = 23{,}000$.

and produces a high Nusselt number on the lower wall as well. Considering the existing scatter in the experimental data for the simpler case of the flat plate, the $v^2 - f$ predictions show very good agreement with the experiment. Let us note that heat transfer rates in the stagnation region are similar on top of the pedestal to the flat plate; thus, stagnation Nusselt number correlations obtained for the plate may be used in the case of a chip. However, if local information is needed, the presence of a minimum heat transfer coefficient, instead of a maximum for the flat plate, emphasizes the need for CFD in more complex geometries.

3.2. Influence of Re number

Turbulence models are sometimes fitted to a given test-case, at a given Reynolds number and might give much worse results when flow conditions are changed. Thus, it is essential to check the range of validity of the accurate results obtained by the $v^2 - f$ model in the previous section for $\mathrm{Re} = 23{,}000$. The dependence on the nozzle-to-plate distance has already been shown to be well captured by the model. Fig. 7 presents the stagnation Nusselt number obtained for different flow rates (i.e. $\mathrm{Re} = 23{,}000$; 50,000; 70,000). The experimental data from Lytle and Webb (1994) and Yan (1993) are plotted on the same graph and a line of best fit to the data has been drawn for comparison purposes. One can see that the dependence on Reynolds number, predicted by the $v^2 - f$ model, is in excellent agreement with the experimental data. In particular, the quasi-laminar correlation $\mathrm{Nu}_{\mathrm{stag}} \propto \mathrm{Re}^{0.5}$ observed experimentally has been obtained accurately. Of course, the Re number is high enough to assure a turbulent regime; for instance, Viskanta (1993) noted that heat transfer rates are 1.4–2.2 times as high as in laminar flow. Moreover, a $v^2 - f$ correlation, showing the Nusselt number evaluated at 6 jet diameters away from the stagnation point, for different jet-to-plate distances, has been added to Fig. 7. In agreement with a statement in Jambunathan et al. (1992), the $v^2 - f$ heat transfer at this location is nearly independent of nozzle-to-plate spacing. Moreover, the $v^2 - f$ model predicts a Nusselt number dependence on $\mathrm{Re}^{0.77}$, in good agreement with previous experiments, which have established a Re exponent in the range of 0.7–0.85 (see Jambunathan et al., 1992; Viskanta, 1993).

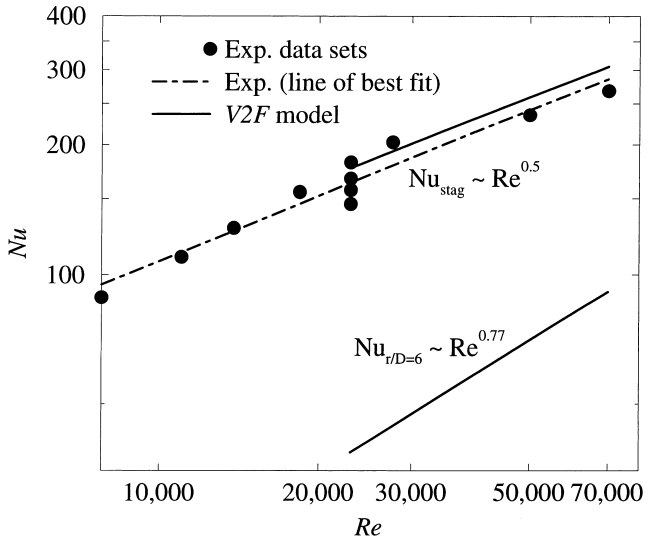

Fig. 7. Dependence of stagnation Nusselt number on Reynolds number for the impinging jet on the flat plate at $H/D = 6$, insert shows simulated dependence of Nusselt number at $r/D = 6$ on Reynolds number.

4. Computational results

4.1. Flow physics

The anomalously high Nusselt number predicted by the $k - \varepsilon$ model can be attributed to erroneous physics. The impinging potential core of the jet contains low levels of turbulence and this should remain relatively low in the vicinity of the stagnation point. The $v^2 - f$ predictions are consistent with this expectation. However, the $k - \varepsilon$ model generates a spurious production of kinetic energy in the impinging region, as depicted in Fig. 8. This figure shows contours of k, as predicted by the two models. Excessive production of turbulence is believed to be responsible for the $k - \varepsilon$ model overpredicting the stagnation point Nusselt number. (Some modifications to the $k - \varepsilon$ model have been proposed to remove the anomolous turbulent kinetic energy, such as Launder and Kato, 1993). Behnia et al. (1998) have compared flow field predictions to measurements by Cooper et al. (1993), confirming that the turbulent intensity is more accurately predicted by $v^2 - f$ and that it is greatly overpredicted by $k - \varepsilon$. Mean flow predictions can also be found in that reference.

Some investigators (e.g. Lee et al., 1995; Garimella and Rice, 1995; Colucci and Viskanta, 1996) have attributed the secondary maximum Nusselt number (see Fig. 3) to a transi-

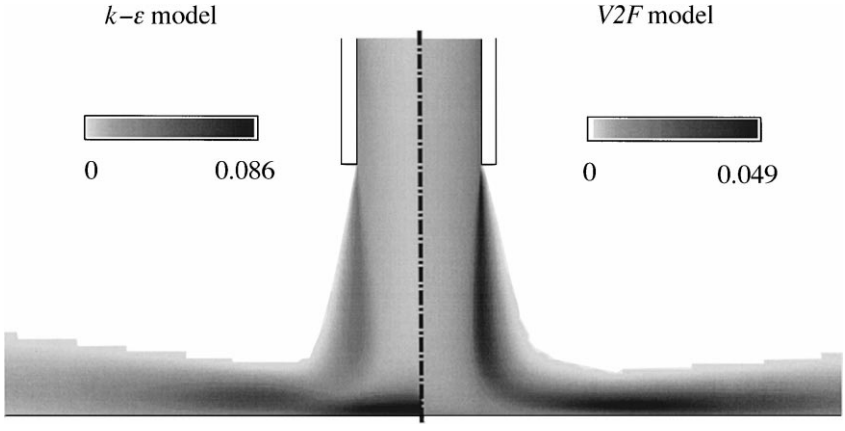

Fig. 8. Shaded contours of turbulent kinetic energy for the impinging jet on the flat plate at $H/D = 2$ and $\mathrm{Re} = 23{,}000$.

tion from a laminar to turbulent boundary layer in the wall jet region. This is not supported by the measurements of Lytle and Webb (1994), who note that there are relatively high levels of turbulence even in the stagnation region. It is believed that a radial increase in the turbulent kinetic energy away from the stagnation point is responsible for this local increase of Nu. This was observed by Lytle and Webb and is predicted by the $v^2 - f$ model, as illustrated in Fig. 8. The increase in the turbulent energy is produced by high shear in the region of streamline convergence, away from the stagnation point. The physical phenomenon involved in this augmentation of turbulent energy is radically different than what can be found around airfoils for example, where the incident flow is first laminar and then undergoes transition to turbulence. Despite the $Re^{0.5}$ correlation of Nusselt number, the flow is not laminar in the stagnation region. Here, the boundary layer evolves from a low level of turbulence to a high turbulence level along the solid surface. Note that this secondary phenomenon becomes larger when Re increases or H/D decreases.

4.2. Influence of confinement

All the previous computations have been performed for an unconfined geometry. Industrial applications, especially in electronic cooling, often require the jet to be confined by a solid boundary at the level of the nozzle exit. Numerous experiments have been conducted to study the effect of confinement on jet impingement heat transfer. The main aim was to know whether the physics and correlations of unconfined geometries could be applied to confined geometries. Obot et al. (1982) concluded that there was between a 5% and 10% reduction in the average heat transfer rate when confinement was added. Again, comparisons to other experiments are difficult to establish, since jet outlet profiles or experimental conditions differ; moreover, no experimental data are available for a fully developed jet, exiting from a long pipe. Since $v^2 - f$ simulations gave satisfactory results in the unconfined geometry, we believe that the model is accurate enough to undertake a numerical study.

Several computations were performed with a wall at the nozzle exit. We varied the nozzle-to-plate distance, and the local heat transfer rates are compared to the results obtained with an unconfined geometry. Fig. 9 shows the Nusselt number distribution for different H/D. For a high enough nozzle-to-plate spacing, the confinement has no effect on the heat transfer rate. The presence of a top wall creates a recirculation (Fig. 10), but its influence on the wall heat transfer is weak; indeed, no significant changes are observed when H/D is greater than unity. For $H/D < 0.5$, the Nusselt number distribution noticeably departs from the free jet case. As has been found in experiments, the average heat transfer rate is lower for the confined case. This may be attributed to two causes: firstly, the Nusselt number is evaluated with the jet temperature as the reference. At high radial distances, this temperature might not be the same as the ambient temperature in the confined case, since the fluid gets heated in the whole confined section. To minimize this effect, we imposed an isothermal boundary condition on the top wall, in order to keep the jet temperature as a meaningful reference.

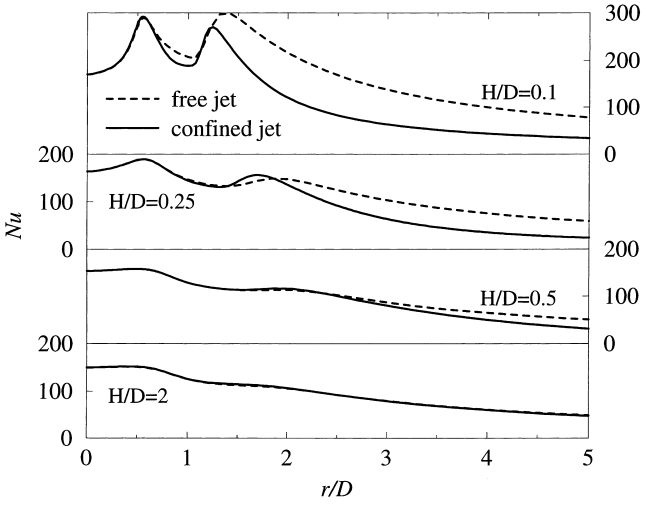

Fig. 9. Comparison of Nusselt number distributions for $H/D = 2$, 0.5, 0.25 and 0.1 between the confined and unconfined flat plate configurations, $Re = 23{,}000$.

Secondly, the top wall introduces a resistance to the flow that gets larger when H/D decreases. Entrainment of the external fluid by the jet diminishes, decreasing the global efficiency of the impinging jet heat transfer. The friction coefficient distribution, shown in Fig. 11, demonstrates that the influence of confinement on surface heat transfer is very similar to its effect on the flow itself. No fluid is entrained from the upper boundary because of the confinement wall. The mass flux decreases, and the bulk velocity is much lower in the confined case.

Fig. 12 also shows the presence of a more pronounced and active recirculation at the nozzle exit, located closer to the target plate. This has a stronger influence on the flow and heat transfer distribution than in the unconfined case. Nevertheless, even for very low H/D (as low as 0.1), neither the heat transfer rates nor the flow in the stagnation region is influenced by confinement. Up to a radial distance of 0.5 jet diameters from the stagnation point, the Nu and C_f distributions stay unchanged, whether the jet is confined or not. This is partially confirmed by Garimella and Rice (1995) who noted that, for $H/D > 2$, confinement had little effect on heat transfer at the stagnation point. A primary peak develops at $r/D \simeq 0.5$ as H/D decreases. This peak corresponds to the acceleration of the local flow due to the decrease of the passage area, which occurs for $H/D < 0.25$. Its location is fixed, in good agreement

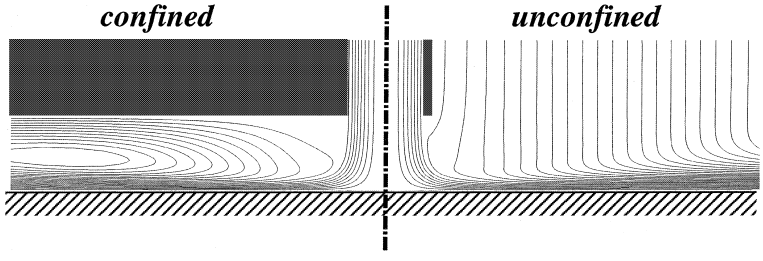

Fig. 10. Comparison of streamlines for $H/D = 1$ and $Re = 23{,}000$ between the confined and unconfined flat plate configurations.

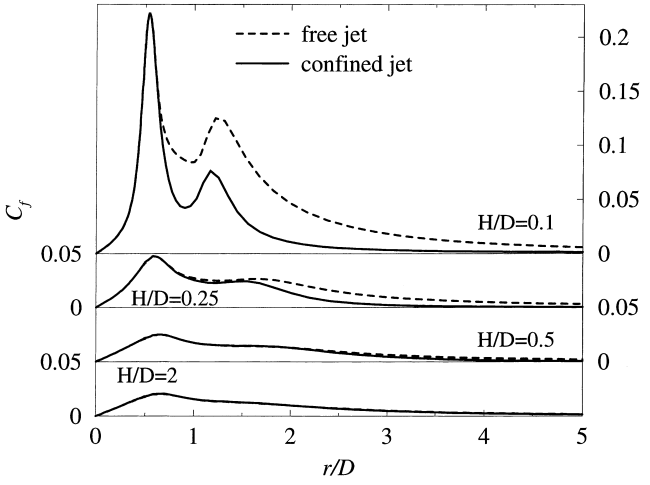

Fig. 11. Comparison of friction coefficient distribution for $H/D = 2$, 0.5, 0.25 and 0.1 between the confined and unconfined flat plate configurations, Re = 23,000.

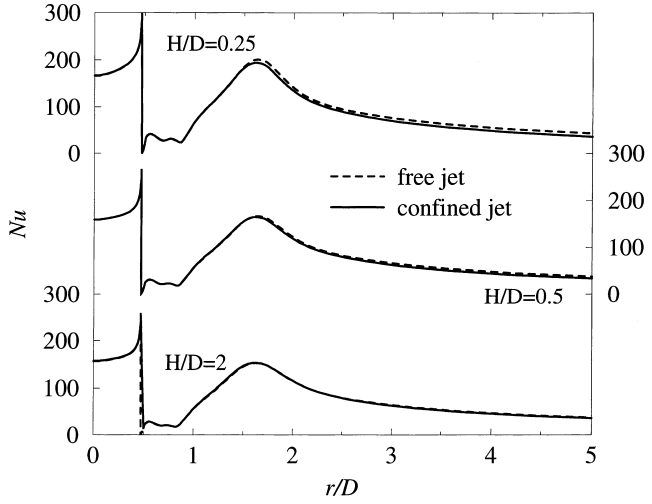

Fig. 13. Comparison of Nusselt number distributions for $H/D = 2$, 0.5 and 0.25 between the confined and unconfined pedestal configurations, Re = 23,000.

with the Colucci and Viskanta experiment (1996). However, secondary peak is also created. It moves toward the axis of symmetry when the nozzle-to-plate distance is decreased. Again, such a behavior is in qualitative agreement with experiment (Colucci and Viskanta, 1996).

Similar computations have been performed for the case of a wall-mounted heated pedestal. One can see in Fig. 13 that the influence of confinement in this geometry is much less than for the flat plate. Even for $H/D = 0.25$, heat transfer rates remain unchanged. The diameter of the pedestal is slightly smaller than the jet diameter: thus, the previous flat plate results lead one to expect little confinement effect on top of the pedestal ($r/D < 0.5$). Downstream, on the base plate, the top wall is at a normalized distance of more than one jet diameter (i.e., $H/D + 1/1.06$). This distance is too high to expect any significant change in the heat transfer rates. Similarly, the recirculation region of Fig. 1(b), which is driven by the jet itself, is less affected by the confinement.

From these results we conclude that confinement does not have a significant impact on the wall heat transfer coefficient unless the jet-to-target spacing is low (i.e. $H/D < 0.25$). The average Nusselt number decreases with confinement, but the local heat transfer distribution in the stagnation region ($r/D < 0.5$) is not modified; unconfined impinging jet stagnation Nusselt number correlations can be used in many cases.

4.3. Influence of nozzle-exit profiles

As previously mentioned, a large scatter exists in experimental data on impinging jet heat transfer rates. In the previous section the effect of confinement was shown to be significant only for very low nozzle-to-plate distances, and only away from the stagnation region ($r/D > 0.5$). Recent experiments by Garimella and Nenaydykh (1996) study the effect of nozzle length-to-diameter ratio on heat transfer. The variation of the length of the nozzle, l, has a direct effect on the nozzle-exit profiles, if parameters like Re and H/D are kept constant. Garimella and Nenaydykh found that for small aspect ratios ($1 < l/D < 4$), the heat transfer coefficients were smaller than for fully developed flow. Their study extended up to a nozzle length of 12 diameters, and Nu differences were on the order of 10–15%. Larger differences are expected for smaller l/D, since pipe flow profiles need at least a distance of 50 diameters to become fully developed.

In this section, $v^2 - f$ computational results are presented with different inlet pipe-profiles. Short pipe calculations were performed to generate boundary layer type mean flow and turbulence profiles. The pipe was long enough to allow a turbulent boundary layer (TBL) to develop. The bulk velocity (U_b) is kept constant so that a fair comparison can be made. Some characteristic parameters (momentum and displacement

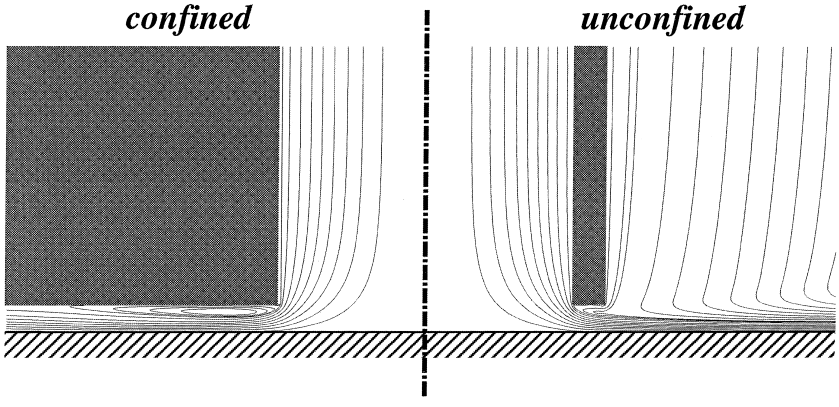

Fig. 12. Comparison of streamlines for $H/D = 0.1$ and Re = 23,000 between the confined and unconfined flat plate configurations.

Table 1
Characteristic parameters of nozzle profiles one diameter upstream of jet-exit

	U_c/U_b	Re_θ	Re_δ	$Tu_c(\%)$
FD	1.21	944	1160	6.7
TBL1	1.06	278	465	1.0
TBL2	1.06	276	463	6.5

Reynolds numbers, Re_θ and Re_δ, normalized centerline velocity U_c/U_b and turbulence levels, Tu) of the three different nozzle exit conditions are presented in Table 1. These conditions correspond to the fully developed (FD) pipe flow used in Section 3.2, and to two different boundary layers (TBL1 and TBL2).

Fig. 14 presents the heat transfer coefficient for the three different profiles. The unconfined jet at $Re = 23{,}000$ and $H/D = 2$ has been chosen for these simulations. In contrast to the confinement effect, the influence of the nozzle exit profiles is largest close to the stagnation line ($r/D < 2$) and is quite strong. The TBL profiles result in a 15–30% decrease in stagnation heat transfer rate, in qualitative agreement with Garimella and Nenaydykh (1996): the TBL cases correspond to a shorter pipe-length than the FD case. Moreover, the qualitative appearance of the Nu distribution is modified, with the emergence of a double-peak. The secondary peak at $r/D \simeq 2$, which is the only peak for the FD case, becomes more pronounced for the TBL cases. The primary local maximum, that appears closer to the stagnation line, is fundamentally different from the peak described in Section 3.2. In the present configuration there is no increase of mean velocity due to confinement. The primary peak is believed to be due to the higher mean velocity gradients in the boundary layers at the nozzle-exit.

The two TBL profiles shows, as expected, that level of turbulence in the core region of the jet has a strong influence on stagnation heat transfer. Nevertheless, for similar turbulence levels, the FD case stagnation Nusselt number is still 15% higher than the TBL2 case. In fact, for small H/D, the pre-impingement potential core of the jet is largely inviscid (Garimella and Nenaydykh, 1996), so turbulence is not expected to be the main governing parameter in this part of the flow. Note

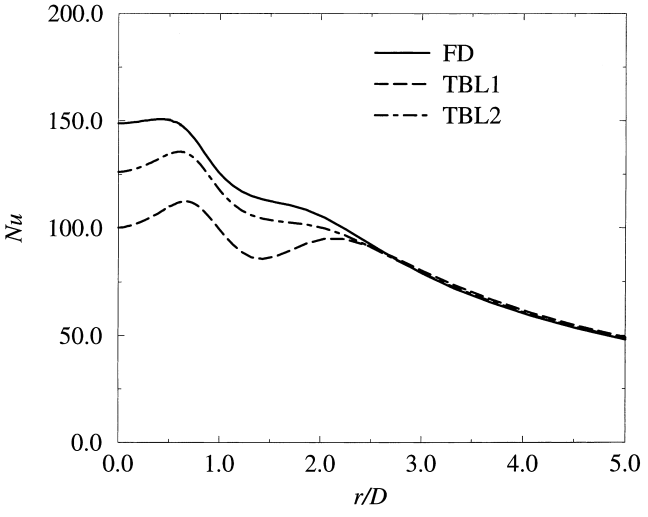

Fig. 14. Comparison of local heat transfer distribution for $H/D = 2$ and $Re = 23{,}000$ evaluated with different nozzle-exit velocity profiles (for legends see Table 1).

also that even laminar computations indicate that impingment heat transfer rates are strongly dependent on jet-exit velocity profiles (Schafer et al., 1992; Al-Sanea, 1992). In the present case, the FD profiles show a 15% increase in centerline velocity, relative to the TBL profiles. This difference in local velocity still exists in the stagnation region and explains the different levels of heat transfer.

Clearly, nozzle-exit profiles have a strong influence on the heat transfer rates, especially in the stagnation region, up to a radial distance of 2 jet diameters, and at small nozzle-to-plate distances, for which the free jet has no time to develop. Differences in velocity profiles are as important a parameter as differences in jet-core turbulence intensity. Any data correlation becomes difficult to use since it is strongly dependent on the experimental jet conditions. For example, swirl and secondary flow in the nozzle might be of significant importance. This highlights the need for accurate CFD computations in industrial design.

5. Concluding remarks

In this study, the $v^2 - f$ turbulence model has been used to evaluate the influence of nozzle-to-target distance, Reynolds number, jet confinement and jet-exit profiles on axisymmetric impinging jet heat transfer. The model was first validated against available experimental data. It was shown to perform very well in a range of H/D and Re, in order to give confidence in its use as a predictive tool.

The effects of confinement and nozzle-exit characteristics were then studied. Confinement was shown to have little effect on the heat transfer coefficient, except for very low nozzle-to-plate distances. By contrast, velocity profiles and the turbulent intensity in the nozzle have a strong influence on the quantitative and qualitative Nu distribution. This partly explains the scatter in the available experimental data. It also shows that data correlations may be erroneous or difficult to use if flow conditions in the nozzle are not known.

Acknowledgements

We thank Professors Baughn, Viskanta, Webb and Yan and Dr. Mesbah for having provided us with their experimental data.

Appendix A

The equations of the $v^2 - f$ model are briefly summarized below. The standard $k - \varepsilon$ type notation is used.

$$D_t U = -\nabla P + \nabla \cdot ((\nu + \nu_t)(\nabla U + \nabla^t U)), \tag{A.1}$$

$$\nabla \cdot U = 0, \tag{A.2}$$

$$D_t k = P - \varepsilon + \nabla \cdot ((\nu + \nu_t)\nabla k), \tag{A.3}$$

$$D_t \varepsilon = \frac{C'_{\varepsilon 1} P - C_{\varepsilon 2}\varepsilon}{T} + \nabla \cdot \left(\left(\nu + \frac{\nu_t}{\sigma_\varepsilon}\right)\nabla \varepsilon\right), \tag{A.4}$$

$$D_t \overline{v^2} = kf - \frac{\overline{v^2}}{k}\varepsilon + \nabla \cdot ((\nu + \nu_t)\nabla \overline{v^2}), \tag{A.5}$$

$$f - L^2 \nabla^2 f = (C_1 - 1)\frac{(2/3 - \overline{v^2}/k)}{T} + C_2 \frac{P}{k}. \tag{A.6}$$

In which

$$v_t = C_\mu \overline{v^2} T; \quad p = 2 v_t S^2; \quad S^2 \equiv S_{ij} S_{ij};$$
$$S_{ij} = \frac{1}{2}\left(\frac{\partial U_i}{\partial x_j} + \frac{\partial U_j}{\partial x_i}\right) \tag{A.7}$$

and the length and time scales are

$$L' = \min\left(\frac{k^{3/2}}{\varepsilon}; \frac{1}{\sqrt{3}\,\overline{v^2} C_\mu \sqrt{2S^2}}\frac{k^{3/2}}{}\right),$$
$$L = C_L \max\left(L'; C_\eta\left(\frac{v^3}{\varepsilon}\right)^{1/4}\right), \tag{A.8}$$

$$T' = \max\left(\frac{k}{\varepsilon}; 6\left(\frac{v}{\varepsilon}\right)^{1/2}\right),$$
$$T = \min\left(T'; \frac{\alpha}{\sqrt{3}\,\overline{v^2} C_\mu \sqrt{2S^2}}\frac{k}{}\right). \tag{A.9}$$

The solid wall no-slip boundary conditions are: $U = 0$, $k = \partial_n k = 0$, $\overline{v^2} = 0$ and $\overline{v^2} = \mathrm{O}(x_n^4)$, x_n being the axis normal to the wall. The $v^2 - f$ constants are given below.

$$C'_{\varepsilon_1} = 1.44(1 + 0.045\sqrt{k/\overline{v^2}}),$$

$$C_\mu = 0.19, \quad C_L = 0.3, \quad C_\eta = 70.0, \quad \alpha = 0.6,$$

$$C_1 = 1.4, \quad C_2 = 0.3, \quad C_{\varepsilon 2} = 1.9, \quad \sigma_\varepsilon = 1.3.$$

The mean temperature equation is

$$D_t \Theta = \nabla \cdot \left(\left(\frac{v}{\mathrm{Pr}} + \frac{v_t}{\mathrm{Pr}_t}\right)\nabla\Theta\right) \tag{A.10}$$

with

$$\mathrm{Pr}_t = \frac{1}{0.5882 + 0.228(v_t/v) - 0.0441(v_t/v)^2[1 - \exp(-5.165 v/v_t)]}.$$

References

Al-Sanea, S., 1992. A numerical study of the flow and heat transfer characteristics of an impinging laminar slot-jet including crossflow effects. Int. J. Heat Mass Transfer. 35, 2501–2513.

Baughn, J., Hechanova, A., Yan, X., 1991. An experimental study of entrainment effects on the heat transfer from a flat surface to a heated circular impinging jet. ASME J. Heat Transfer 113, 1023–1025.

Baughn, J., Mesbah, M., Yan, X., 1993. Measurements of local heat transfer for an impinging jet on a cylindrical pedestal. ASME HTD239, 57–62.

Baughn, J., Shimizu, S., 1989. Heat transfer measurements from a surface with uniform heat flux and an impinging jet. ASME J. Heat Transfer. 111, 1096–1098.

Behnia, M., Parneix, S., Durbin, P., 1998. Prediction of heat transfer in an axisymmetric turbulent jet impinging on a flat plate. Int. J. Heat Mass Transfer 41, 1845–1855.

Colucci, D., Viskanta, R., 1996. Effect of nozzle geometry on local convective heat transfer to a confined impinging air jet. Experimental Thermal and Fluid Science 13, 71–80.

Cooper, D., Jackson, D., Launder, B., Liao, G., 1993. Impinging jet studies for turbulence model assessment–I Flow-field experiments. Int. J. Heat Mass Transfer 36, 2675–2684.

Craft, T., Graham, L., Launder, B., 1993. Impinging jet studies for turbulence model assessment–II. An examination of the performance of four turbulence models. Int. J. Heat Mass Transfer 36, 2685–2697.

Durbin, P., 1991. Near-wall turbulence closure without damping functions. Theoretical and Computational Fluid Dynamics 3, 1–13.

Durbin, P., 1993. A Reynolds-stress model for near-wall turbulence. J. Fluid Mech. 249, 465–498.

Durbin, P., 1996. On the $k - \varepsilon$ stagnation point anomaly. Int. J. Heat and Fluid Flow 17, 89–90.

Garimella, S., Rice, R., 1995. Confined and submerged liquid jet impingement heat transfer. ASME J. Heat Transfer 117, 871–877.

Garimella, S., Nenaydykh, B., 1996. Nozzle-geometry effects on liquid jet impingement heat transfer. Int. J. Heat Mass Transfer 39, 2915–2923.

Jambunathan, K., Lai, E., Moss, M., Button, B., 1992. A review of heat transfer data for single circular jet impingement. Int. J. Heat and Fluid Flow 13, 106–115.

Kays, W.M., Crawford, M.E., 1993. Convective heat and mass transfer, 3rd ed., McGraw-Hill, New York.

Launder, B.E., Kato, M., 1993. Modelling flow-induced oscillations in turbulent flow around a square cylinder. ASME FED. 157, 189–199.

Launder, B., Sharma, B., 1974. Application of the energy-dissipation model of turbulence to the calculation of flow near a spinning disc. Letters in Heat Mass Transfer 1, 131–138.

Lee, D., Greif, R., Lee, S., Lee, J., 1995. Heat transfer from a flat plate to a fully developed axisymmetric impinging jet. ASME J. Heat Transfer 117, 772–776.

Lytle, D., 1990. Air jet impingement heat transfer at low nozzle-to-plate spacings. MS Thesis, Brigham Young University.

Lytle, D., Webb, B., 1994. Air jet impingement heat transfer at low nozzle-plate spacings. Int. J. Heat Mass Transfer 37, 1687–1697.

Martin, H., 1977. Heat and mass transfer between impinging gas jets and solid surfaces. Advances in Heat Transfer 13, 1–60.

Mesbah, M., 1996. An experimental study of local heat transfer to an impinging jet on non-flat surfaces: A cylindrical pedestal and a hemispherically concave surface. Ph.D. Thesis, University of California, Davis.

Obot, N., Mujumdar, A., Douglas, W., 1982. Effect of semi-confinement on impinging heat transfer. Proc. 7th Int. Heat Transfer Conf. 3, 395–400.

Rogers, S., Kwak, D., 1990. Upwind differencing scheme for the time-accurate incompressible Navier-Stokes equations. AIAA Journal. 28, 253–262.

Schafer, D., Ramadhyani, S., Incropera, F., 1992. Numerical simulation of laminar convection heat transfer from an in-line array of discrete sources to a confined rectangular jet. Numerical Heat Transfer 22, 121–141.

Viskanta, R., 1993. Heat transfer to impinging isothermal gas and flame jets. Exp. Thermal Fluid Sci. 6, 111–134.

Webb, B., Ma, C.-F., 1995. Single-phase liquid jet impingement heat transfer. Advances in Heat Transfer 26, 105–217.

Yan, X., 1993. A preheated-wall transient method using liquid crystals for the measurement of heat transfer on external surfaces and in ducts. Ph.D. Thesis, University of California, Davis.